Eur. Phys. J. B **72**, 521–529 (2009)
DOI: 10.1140/epjb/e2009-00391-0

THE EUROPEAN PHYSICAL JOURNAL B

Regular Article

Donor-impurity related binding energy and photoinization cross-section in quantum dots: electric and magnetic fields and hydrostatic pressure effects

M.G. Barseghyan[1], A.A. Kirakosyan[1], and C.A. Duque[2,a]

[1] Department of Solid State Physics, Yerevan State University, Al. Manookian 1, 0025 Yerevan, Armenia
[2] Instituto de Física, Universidad de Antioquia, AA 1226, Medellín, Colombia

Received 8 April 2009 / Received in final form 29 August 2009
Published online 20 November 2009 –

Abstract. We have studied the behavior of the binding energy and photoionization cross-section of a donor-impurity in cylindrical-shape GaAs-$Ga_{0.7}Al_{0.3}As$ quantum dots, under the effects of hydrostatic pressure and in-growth direction applied electric and magnetic fields. We have used the variational method under the effective mass and parabolic band approximations. Parallel and perpendicular polarizations of the incident radiation and several values of the quantum dot geometry have also been considered. Our results show that the photoionization cross-section growths as the hydrostatic pressure is increased. For parallel polarization of the incident radiation, the photoionization cross-section decreases when the impurity is shifted from the center of the dot. In the case of perpendicular polarization of the incident radiation, the photoionization cross-section increases when the impurity is shifted in the radial direction of the dot. For on-axis impurities the transitions between the ground state of the impurity and the ground state of the quantum dot are forbidden. In the low pressure regime (less than 13.5 kbar) the impurity binding energy growths linearly with pressure, and in the high pressure regime (higher than 13.5 kbar) the binding energy growths up to a maximum and then decreases. Additionally, we have found that the applied electric and magnetic fields may favor the increase or decrease in binding energy, depending on the impurity position.

PACS. 71.55.Eq III-V semiconductors – 78.67.Hc Quantum dots

1 Introduction

Low-dimensional semiconductor heterostructures, such as quantum wells (QW), quantum-well wires (QWW), and quantum dots (QD), have received special attention in the past three decades. The reason for this resides in the numerous potential applications to sensors, optoelectronic systems, control systems, single-electron transistors, and infrared photo-detectors. In the case of QWs and QWWs, it is known that for each state related to a special direction of confinement, it is possible to associate a continuum of states – this continuum arising from the free-particle solutions corresponding to directions in which there is no confinement. However, in the case of QDs, only a discrete set of states – similar to those of a single atom – are present, due to confinement in all directions of space. Subbands (in the case of QW and QWW), and sets of discrete states (in the case of QD), and their interactions can be controlled by using electric and magnetic fields, changes in the incident laser radiation, hydrostatic pressure, hydrostatic-pressure induced $\Gamma-X$ mixing, or simply by including shallow-donor and shallow-acceptor impurities that dope the quantum system.

Many works related to shallow-impurities states in QW [1–9], QWW [10–15], and QD [16–26] have been reported recently. In almost all the references cited above, the calculations have been made in the effective-mass approximation and using variational techniques. In general, these works provide a good interpretation of experimental results associated with effects such us geometrical confinement, applied electric and magnetic fields, crossover between the different conduction bands induced by hydrostatic pressure, and temperature, among others. Applied electric fields and a finite increase in temperature are two useful ways, to obtain red-shifts in the optical absorption and photoluminescence spectra [27,28]. In the case of blue-shifts, it is useful to consider, for example, the effects of applied magnetic fields and hydrostatic pressure [29–33] to tune the value of the electrical field for which the exciton-peak energy transition corresponds to

[a] e-mail: cduque@fisica.udea.edu.co

spatially direct or indirect excitons [34–36]. The applied electromagnetic field can destroy a preexisting symmetry, or restore a broken symmetry. In this manner, in the case of shallow impurities, the binding energy can be increased or decreased, depending on the direction of the applied electric and magnetic fields, and on the impurity position in the heterostructures [8,10]. In the case of magnetic fields, generally their contribution is to increase the binding energy due to the reductions in the radius of the cyclotron orbits with the applied field. Associated with the decreasing of the static dielectric constant with hydrostatic pressure, in semiconductors such as GaAs and $Ga_{1-x}Al_xAs$ usually hydrostatic pressure implies an increasing in binding energy due to the reduction of the carriers screening to the impurity center [9,14]. However, in the high hydrostatic pressure regime, over the $\Gamma - X$ crossover for the barrier material, the binding energy decreases as the hydrostatic pressure increases, because of the lowering of the barrier potential which confines the carriers inside the heterostructure.

Theoretical studies about the photoionization cross-section (PCS) in low dimensional semiconductor systems have been the subject of great interest, due to its importance to understand the optical properties of confined carriers and to characterize the impurity states in the heterostructure. Among the different parameters to be considered when the PCS is calculated, we can mention: 1) the confinement degree (2D in QW, 1D in QWW, and 0D in QD) [37–39]; 2) the energy and polarization of the incident photon; 3) the shape and geometrical dimensions of the heterostructures; 4) the presence of applied electric [40] and/or magnetic fields [41–43], and 5) hydrostatic pressure and temperature [39]. All of them are largely responsible for changes in the threshold energy for transitions from the initial impurity states to final confined states of the carriers, red- and blue-shifts in the structures of the PCS, and widening of the peaks in the line-shape of the PCS. Particularly, in the case of QDs, there are some calculations about PCS for square, cylindrical, and spherical geometries and take into account effects such us hydrostatic pressure and applied magnetic field [44–50]. Sali et al. [44] and Ham et al. [45,46] have calculated the PCS in QDs for on-center (on-axis) and off-center (off-axis) impurities, and show that, depending on the impurity position and the polarization of the incident radiation, new possibilities are allowed for selection rules. They have also shown that, whereas the PCS depends on the photon energy, this dependence is dramatically influenced by dot size. They showed that the photon energy at which the PCS reaches a maximum is equal to the photoionization threshold energy for any direction of the incident light polarization. Correa et al. [47,48] and Barseghyan et al. [50] studied on-axis (on-center) impurities in the cylindrical (spherical) QD; they found also that PCS diminishes as the dimension of the QD heterostructure increases. In spite of these works, there are no systematic studies concerning the combined effects of hydrostatic pressure, applied electric and magnetic field, and polarization of the incident radiation on the donor-related PCS in cylindrical QDs with finite potential barriers in the radial direction and no systematic study is known about impurities located at all possible regions of the QD.

In the present work we extend our previous one [50] and we perform a predictive study of the hydrostatic pressure and applied electric and magnetic field effects on the donor-impurity-related binding energy and PCS in cylindrical-shape GaAs-$Ga_{1-x}Al_xAs$ QDs considering parallel and perpendicular polarizations of the incident radiation and impurities located both on-axis and off-axis inside the heterostructure. Our study about impurities suggests the possibility of extending the allowed selection rules for each polarization of the incident radiation. The effective-mass and parabolic-band approximations have been incorporated within a variational procedure. In Section 2 we present the theoretical framwork. Our results are presented and discussed in Section 3, and Section 4 is for conclusions.

2 Theoretical framework

In the effective-mass approximation the Hamiltonian for a hydrogenic impurity in a GaAs-$Ga_{1-x}Al_xAs$ QD under the influence of applied hydrostatic pressure (P), electric (F) and magnetic (B) fields in the z-direction, is given by

$$H = \frac{1}{2}\left(\widehat{\overrightarrow{p}} + \frac{e\overrightarrow{A}}{c}\right)\frac{1}{m(z,P,T)}\left(\widehat{\overrightarrow{p}} + \frac{e\overrightarrow{A}}{c}\right) + |e|Fz + V(\rho,z,P,T) - \frac{e^2}{\varepsilon(P,T)\,r}, \quad (1)$$

where $\overrightarrow{A}$ is the vector potential and $r = \left[|\overrightarrow{\rho} - \overrightarrow{\rho_i}|^2 + (z - z_i)^2\right]^{\frac{1}{2}}$ is the distance from the carrier to the impurity site [with $(z_i, \overrightarrow{\rho_i})$ and $(z, \overrightarrow{\rho})$ the impurity and electron coordinates, respectively]. Here $m(z,P,T)$ is the z-, pressure-, and temperature-dependent conduction effective mass and $\varepsilon(P,T)$ is the pressure- and temperature-dependent static dielectric constant. They are given by [51]

$$m(z,P,T) = \begin{cases} m_w(P,T), \text{ if } |z| \le L(P)/2, \\ m_b(P,T), \text{ if } |z| \ge L(P)/2, \end{cases} \quad (2)$$

and

$$\varepsilon(P,T) = 12.74 \times \exp(-1.67 \times 10^{-3}\,\text{kbar}^{-1}P) \times \exp\left[9.4 \times 10^{-5}\,\text{K}^{-1}(T - 75.6\,\text{K})\right], \quad (3)$$

with

$$m_w(P,T) = \left[1 + \frac{15020\,\text{meV}}{E_g(P,T)} + \frac{7510\,\text{meV}}{E_g(P,T) + 341\,\text{meV}}\right]^{-1} m_0, \quad (4)$$

$$m_b(P,T) = m_w(P,T) + 0.083\,x\,m_0, \quad (5)$$

$E_g(P,T)$ the bulk GaAs bandgap, given by:

$$E_g(P,T) = \left(1519 + 10.7\,\mathrm{kbar}^{-1}\,P - \frac{0.5405\,\mathrm{K}^{-1}\,T^2}{T + 204\,\mathrm{K}}\right)\ \mathrm{meV}, \quad (6)$$

m_0 the free electron mass, and x (=0.3 in this work) the alloy concentration. The dielectric constant mismatch effects in GaAs-$Ga_{1-x}Al_xAs$ QWs have been reported and indicate that the main effects occur for small well widths and high Al concentration [52]. Following Raigoza et al. [51] we have used the same GaAs dielectric constant along the whole heterostructure. $V(\rho,z,P,T)$ is the confining potential, which is given by [3,4]

$$V(\rho,z,P,T) = \begin{cases} 0, & \text{if } \rho \le R(P),\ |z| \le L(P)/2, \\ V_0(P,T), & \text{if } \rho \ge R(P),\ |z| \le L(P)/2, \\ \infty, & \text{if } |z| \ge L(P)/2, \end{cases} \quad (7)$$

where

$$V_0(P,T) = \begin{cases} \Gamma_b^{(P,T)} - \Gamma_w^{(P,T)}, & P \le P_1, \\ X_b^{(P,T)} - \Gamma_w^{(P,T)} + S_0\,x\,\frac{P-P_1}{P}, & P_1 < P \le P_2, \end{cases} \quad (8)$$

and P_1 (=13.5 kbar) is the crossover pressure between the X_b and the Γ_b conduction bands, P_2 (=35 kbar) is the crossover pressure between the X_b and the Γ_w conduction bands, and T (=4 K in the present work) is the system temperature. S_0 (=250 meV) [3,4] is an adjustable parameter used to fit the predicted energy at P_1 with the experimental result. It is important to clarify that in this work we have followed the model of Elabsy [3,4] by which the effect of the $\Gamma - X$ crossover between the bands of the barrier material, induced by the hydrostatic pressure, is described by the pressure dependence of the height of the finite-potential barriers that confine the carriers inside the heterostructure. Other methods, much more complex, have previously been implemented [2,53–59]. In equation (7), $R(P)$ and $L(P)$ give the pressure-dependent radius and length of the cylindrical QD, and can be obtained by the hydrostatic pressure dependence of the fractional change in volume of the heterostructure [15,60].

To describe the effect of impurity, we used the variational method. The trial function for the ground state of the impurity is written as the product between the first sub-band, associated with the electron in the heterostructures, and a 1s-like hydrogenic function, of spherical character. In the present work, the 1s-like hydrogenic function depends on only one variational parameter ($e^{-\alpha r}$). This type of variational function has been widely used to calculate the binding energy of shallow impurities and excitons, the impurity- and exciton related optical absorption and photoluminescence spectra, and the impurity-related PCS, all of them in low dimensional systems such us QW, QWW, and QD [1–50]. In all these previous references, the authors have considered a wide range of external effects such as electric and magnetic fields arbitrarily oriented in the herostructure, and hydrostatic pressure and multiple positions of the impurity within the heterostructures. Comparisons between these variational calculations with the available experimental findings have been reasonable and therefore, we adopt this scheme in our work. Accordingly we have chosen, as the variational ground impurity state, the following function [61]:

$$\Psi_i(\rho,\varphi,z,\alpha) = N_i\,\Upsilon_{10}(\rho)\,\Phi_1(z)\,e^{-\alpha r}, \quad (9)$$

where N_i is a normalization constant, α is the variational parameter,

$$\Upsilon_{10}(\rho) = \begin{cases} G_1 \times F\left[-\frac{m_w(P,T)E_{10}a_H^2}{\hbar^2} + \frac{1}{2}, 1, \frac{\rho^2}{2a_H^2}\right], & \rho \le R(P), \\ U\left[-\frac{m_b(P,T)(E_{10}-V(P,T))a_H^2}{\hbar^2} + \frac{1}{2}, 1, \frac{\rho^2}{2a_H^2}\right], & \rho > R(P), \end{cases} \quad (10)$$

and $\Phi_1(z) = Ai(Z) + G_2 \times Bi(Z)$ inside the QD region and zero elsewhere. (F, U), and (Ai, Bi) are the degenerate hypergeometric and Airy functions, respectively, a_H is the magnetic length, G_1 and G_2 are constants obtained from continuity condition of the wave function in the interfaces, and $Z = \left[2m_w(P,T)eF/\hbar^2\right]^{1/3}[z - E_{z1}/(eF)]$. Here E_{10} and E_{z1} are the ground-state energies associated with the ρ and z confinements. The impurity ground-state energy is defined as

$$E_i = \langle \Psi_i(\rho,\varphi,z,\alpha_{\min})|H|\Psi_i(\rho,\varphi,z,\alpha_{\min})\rangle, \quad (11)$$

where $\alpha_{\min}$ is the value of α corresponding to the minimum of E_i. The impurity binding energy is defined as

$$E_b = E_0 - E_i, \quad (12)$$

where E_0 is the ground-state electronic energy without the impurity. We study only electric fields below 100 kV/cm. The electron-impurity system always corresponds to a bound system [62] and that is why the model with the trial wave function that we used is a good choice to describe the Stark effect.

It is clear that our variational function gives a better account of the impurity effects when the QD is not under the influence of applied electric field and when the impurity is located at the center of the QD. In this case, both the axial and azimuthal symmetries are preserved. For QD large sizes the variational wave function is not very different from that for the exact spherically symmetric solution of the problem under study. To determine the quality of the trial wave function described above, we have calculated the dispersion of energy ($\Delta E = [\langle H^2\rangle - \langle H\rangle^2]^{1/2}$). For all situations reported in this paper $\Delta E < 3\%$, E_b. These results let us believe that the values obtained for $\langle z\rangle$ and $\langle \rho\cos\varphi\rangle$, between the initial and final states involved in the PCS, will be reasonably well described. Because our family of variational wave functions contains the exact solution of the two- and three-dimensional hydrogenic atom, it is understandable why when in our calculations we take $L \to 0$ with $R \to \infty$ or $L \to \infty$ with $R \to \infty$

the results are $E_b = 4$ effective Rydberg with $\Delta E = 0$ or $E_b = 1$ effective Rydberg with $\Delta E = 0$, respectively. Another type of variational functions, with a larger number of variational parameters could be implemented to further describe the breaking of spherical symmetry associated with the cylindrical shape of the QD where the carriers are confined. Additionally, a much more elaborate calculation would consider the exact solution of the problem in which the wave function for the correlated system is written as a linear combination of the eigenfunctions of the Hamiltonian without the Coulomb interaction. Moreover, numerical solutions with methods for solving differential equations could improve the numerical results reported here. In the problem considered in this work we have taken into account several approximations such us: 1) the effective mass with parabolic conduction bands; 2) the electric field is only applied in the quantum dot region; 3) an infinite confinement potential in the z direction; and 4) we have not taken into account the effects of an image charge associated with the difference in the dielectric constant between the QD and barrier materials in the radial direction. With these approaches, it is clear that a method of exact solution of the Schrödinger equation, or a variational calculation with a trial function with a large number of variational parameters would be beyond the objectives of this research.

The PCS describing the transitions from the impurity ground-state $|\Psi_i\rangle$ to the final state $|\Psi_f\rangle$ in the dipole and effective-mass approximations is given by [39,41,43]

$$\sigma(\omega, P, T) = \Omega \sum_f \left| \left\langle \Psi_i \left| \overrightarrow{\zeta} \cdot \overrightarrow{r} \right| \Psi_f \right\rangle \right|^2 \delta\left(E_f - E_i - \hbar\omega\right), \tag{13}$$

where

$$\Omega = \Omega(P,T) = 4\pi^2 \alpha_{_{FS}} \varepsilon_w^{-1/2}(P,T) \hbar\omega \left(\frac{E_{eff}}{\Lambda}\right)^2 \left(\frac{m_w(P,T)}{m_0}\right)^2, \tag{14}$$

$\alpha_{_{FS}} = e^2/(\hbar c)$ is the fine structure constant, $\hbar\omega$ is the photon energy, E_{eff} is the effective electric field on the impurity, Λ is the average field, $\overrightarrow{\zeta}$ is the light polarization vector, m_0 is the free electron mass, and E_f and E_i are the energies of the final and initial states. The final state is the eigenfunction of the Hamiltonian in equation (1) without the impurity potential term (last term at the right) which is given by

$$\Psi_f(\rho, z) = N_f \, \Upsilon_{10}(\rho) \, \Phi_1(z). \tag{15}$$

Here N_f is a normalization constant. We have considered the case in which the polarization vector is directed along the z axis (parallel polarization); in this case the selection rules for the matrix element of the dipole moment indicate that we must consider those transitions from the first impurity state to the ground state of the cylindrical QD. The PCS may then be written as $\Delta \times I_1$ for parallel polarization of the incident radiation and $\Delta \times I_2$ for perpendicular polarization, where

$$\Delta = \Omega \times \frac{\Gamma}{\pi\left[\left(E_b - \hbar\omega\right)^2 + \Gamma^2\right]}, \tag{16}$$

$$I_1 = N_i^2 N_f^2 \left| \int_{-L/2}^{+L/2} \int_0^{\infty} \times \int_0^{2\pi} z \left|\Upsilon_{10}(\rho)\right|^2 \left|\Phi_1(z)\right|^2 e^{-\alpha r} \rho \, d\rho \, dz \, d\varphi \right|^2, \tag{17}$$

and

$$I_2 = N_i^2 N_f^2 \left| \int_{-L/2}^{+L/2} \int_0^{\infty} \times \int_0^{2\pi} \rho \cos\varphi \left|\Upsilon_{10}(\rho)\right|^2 \left|\Phi_1(z)\right|^2 e^{-\alpha r} \rho \, d\rho \, dz \, d\varphi \right|^2. \tag{18}$$

Here Γ (=0.4 meV in this work) is a Lorentzian parameter. According to equation (18), when the polarization vector is directed along the y-axis, the transitions from the ground impurity state to the first band are forbidden. These transitions are forbidden also when the donor impurity is located on the z-axis ($\rho_i = 0$).

3 Results and discussion

In Figures 1–4 we present our results for the binding energy as a function of the hydrostatic pressure in cylindrical-shape GaAs-$Ga_{0.7}Al_{0.3}As$ QDs considering different values of the dot size (R and L), external applied electric and magnetic fields, and donor impurity positions. For the parameters used in the present calculation see, for example, Correa et al. [39] and references therein.

In all cases that we studied, the binding energy increases linearly with pressure up to 13.5 kbar, mainly due to the fact that for this pressure regime the barrier height remains constant. For higher pressure values, the binding energy reaches a maximum and then decreases, because the potential barrier decreases monotonically as the pressure increases. For the complete range of hydrostatic pressure we are considering, the following effects are also observed: 1) the electron-effective mass is an increasing function of pressure, which itself increases the binding energy; 2) the static dielectric constant is a decreasing function of pressure, which itself increases the Coulomb interaction and, consequently, increases the binding energy; and 3) the dimensions of the dot decrease with pressure, and this forces the binding energy to increase or decrease, depending on whether the system is in the high or low confinement regime.

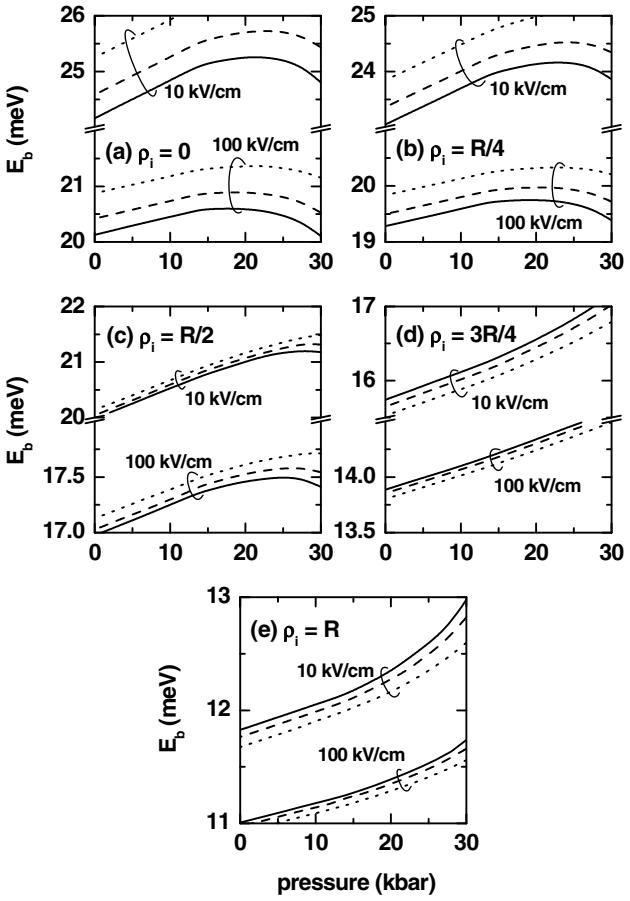

Fig. 1. Binding energy of a donor impurity in cylindrical-shape GaAs-(Ga, Al)As quantum dot ($R = 100$ Å, $L = 200$ Å) as a function of the hydrostatic pressure. Several impurity positions (z_i, ρ_i) have been considered: (0, 0) (a), (0, $R/4$) (b), (0, $R/2$) (c), (0, $3R/4$) (d), and (0, R) (e). Solid, dashed, and dotted lines are for 10 T, 20 T, and 30 T, respectively, for the external applied magnetic field. Results are for two different strengths of the applied electric field, 10 kV/cm and 100 kV/cm.

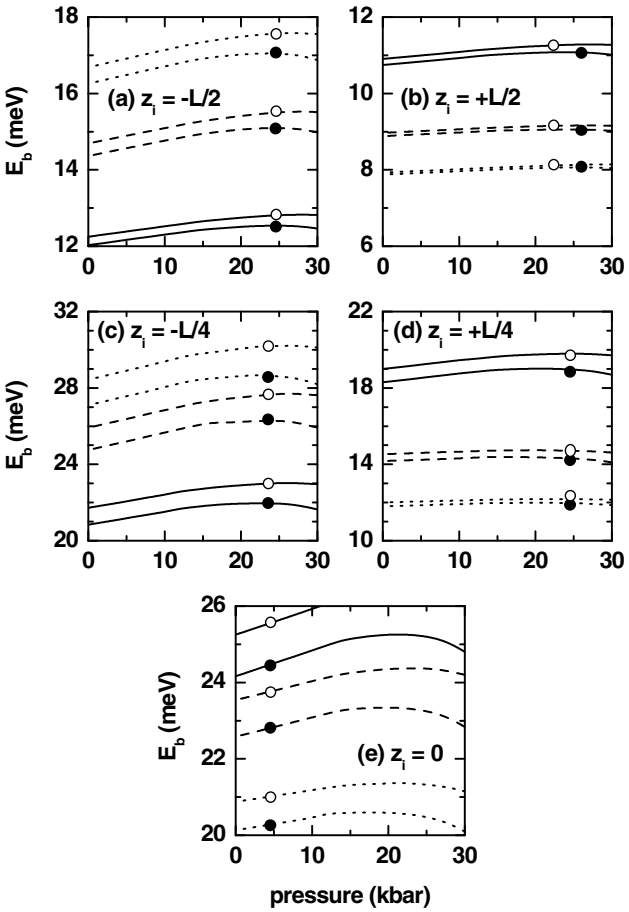

Fig. 2. Binding energy of a donor impurity in cylindrical-shape GaAs-(Ga, Al)As quantum dot ($R = 100$ Å, $L = 200$ Å) as a function of the hydrostatic pressure. Several impurity positions (z_i, ρ_i) have been considered: ($-L/2$, 0) (a), ($+L/2$, 0) (b), ($-L/4$, 0) (c), ($+L/4$, 0) (d), and (0, 0) (e). Solid, dashed, and dotted lines are for 10 kV/cm, 50 kV/cm, and 100 kV/cm, respectively, for the external applied electric field. Solid and open symbols denote, respectively, 10 T and 30 T for the external applied magnetic field.

In Figure 1 we present the hydrostatic pressure dependencies of the binding energy for several values of the applied magnetic field and the radial-impurity coordinate, ρ_i. From Figures 1a–1c it is clear that with increasing magnetic fields the binding energy increases as the carrier is much more localized along the axis of the dot; such effect is more apparent for the smaller values of the radial-impurity coordinate. When the impurity is shifted from the QD axis to $\rho_i = 3R/4$ or $\rho_i = R$, the binding energy decreases with increasing magnetic field, due to the smaller probability for the electron to be near the impurity. In this last case the effect of the applied magnetic field is to localize the carrier along the z-axis of the dot and far from the impurity center, with the corresponding reduction of the binding energy. In Figure 1, the bending of the curves is larger for lower magnetic field induction and lower impurity coordinate values. The bending of these curves can be understood as an effect of the magnetic field pushing the carriers along the axial direction of the dot. For $\rho_i = 3R/4$ or $\rho_i = R$ (see Figs. 1d and 1e) and for fixed values of the impurity coordinate with increasing magnetic field the binding energy decreases. With increasing magnetic field the delocalization of the electron is decreasing (Coulomb interaction is weaker). From Figures 1d and 1e it is clear that with increasing pressure the binding energy increases monotonically (no bending). Because in this case the localization of the electron is caused basically by magnetic field effects, we understand that the behavior of the curves is caused mainly by the increasing of the effective mass with the hydrostatic pressure. Because all the results in Figure 1 are reported for the impurity at $z_i = 0$, with the increasing of the applied electric field also there is an increasing in the expectation value of the electron-impurity distance along the z-direction with the corresponding decreasing of the binding energy, as can be observed by comparing the results at 10 kV/cm and 100 kV/cm.

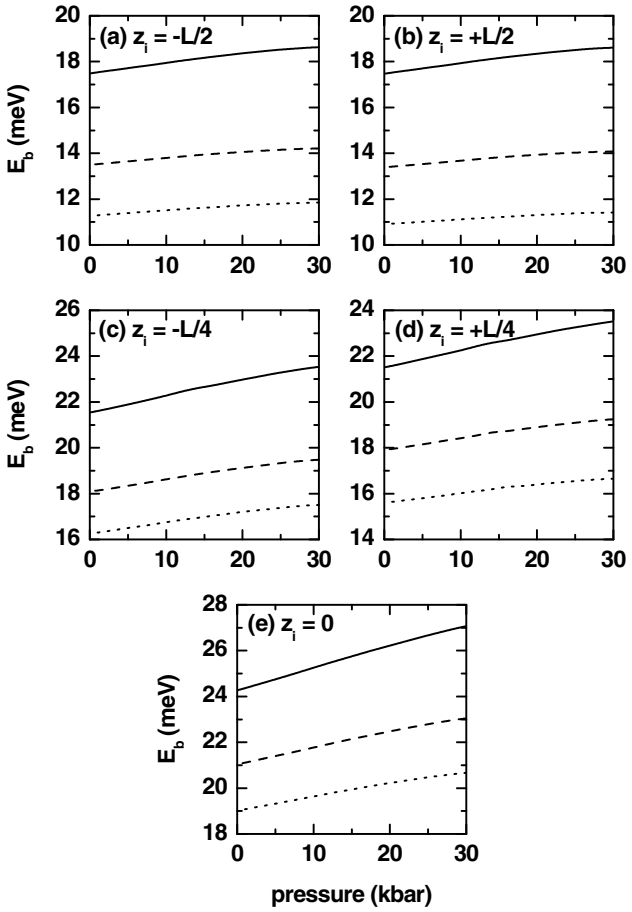

Fig. 3. Binding energy of a donor impurity in cylindrical-shape GaAs-(Ga, Al)As quantum dot ($R = 200$ Å) as a function of the hydrostatic pressure. Several impurity positions (z_i, ρ_i) have been considered: ($-L/2$, 0) (a), ($+L/2$, 0) (b), ($-L/4$, 0) (c), ($+L/4$, 0) (d), and (0, 0) (e). Solid, dashed, and dotted lines are for $L = 50$ Å, $L = 100$ Å, and $L = 150$ Å, respectively. The results are for $B = 10$ T and $F = 10$ kV/cm.

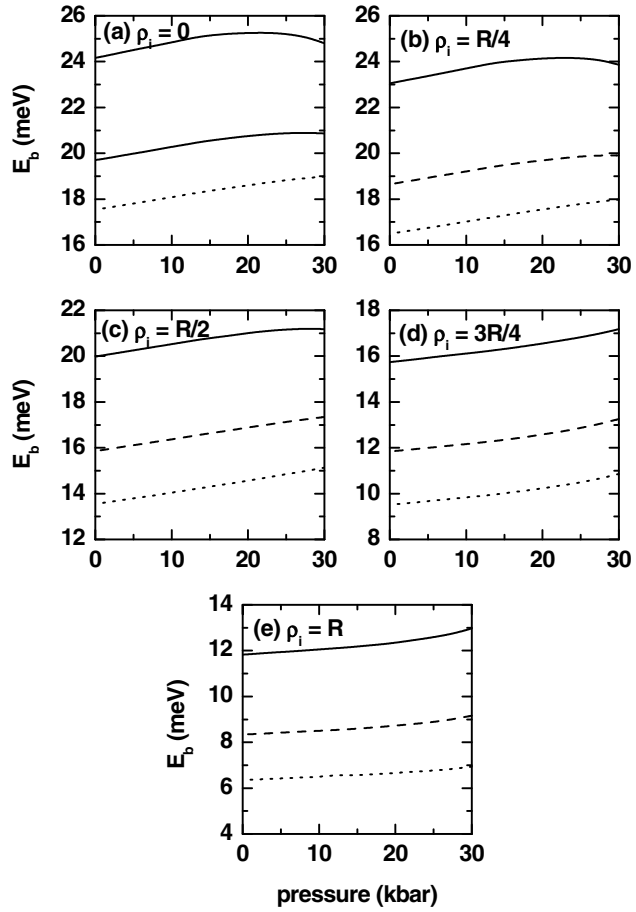

Fig. 4. Binding energy of a donor impurity in cylindrical-shape GaAs-(Ga, Al)As quantum dot ($L = 200$ Å) as a function of the hydrostatic pressure. Several impurity positions (z_i, ρ_i) have been considered: (0, 0) (a), (0, $R/4$) (b), (0, $R/2$) (c), (0, $3R/4$) (d), and (0, R) (d). Solid, dashed, and dotted lines are for $R = 100$ Å, $R = 150$ Å, and $R = 200$ Å, respectively. The results are for $B = 10$ T and $F = 10$ kV/cm.

We calculated the effect of the hydrostatic pressure on the binding energy of a donor impurity located at several axial positions (z_i); we did this for the case of cylindrical-shape QD, and for several values of the applied electric field; our results are displayed in Figure 2. From Figures 2a–2c, when the impurity is shifted from the center of the dot and in the same direction of the applied electric field, it is clear that for fixed values of the impurity coordinate the binding energy decreases with the increasing of the electric field. The explanation of this behavior can be as follows. The electric field forces the electron to leave the impurity, this causes an increasing in the expectation value of the electron-impurity distance, and this is accompanied by a reduction of the Coulomb interaction. When the z_i increases, the localization of electron diminishes and the binding energy decreases. The opposite behavior is observed when the impurity is shifted in the $-z$ direction, as shown in Figures 2a, 2d, and 2e. In this last case, the electric field reduces the electron-impurity distance with the corresponding increasing in the binding energy, and this happens because the infinite potential barrier in $z = -L/2$ repels the wavefunction. Because all the results in Figure 2 are reported for the impurity at $\rho_i = 0$, with the increasing of the applied magnetic field there is a decreasing in the expectation value of the electron-impurity distance along the radial-direction with the corresponding increasing of the binding energy, as can be observed by comparing the results at 10 T and 30 T.

Figures 3 and 4 show the dependencies of the binding energy with the hydrostatic pressure for different values of the cylindrical-shape QD length and radius, respectively. In all cases, and for fixed values of the impurity coordinate, the binding energy decreases when the radius and length are increased. The binding energy decreases due to the reduction of the geometrical confinement. The behavior with the axial and radial impurity positions is in accordance with the physical analysis in Figures 1 and 2.

In Figure 5 we present the impurity-related PCS as a function of hydrostatic pressure in the case of parallel polarization of the incident radiation, for several values

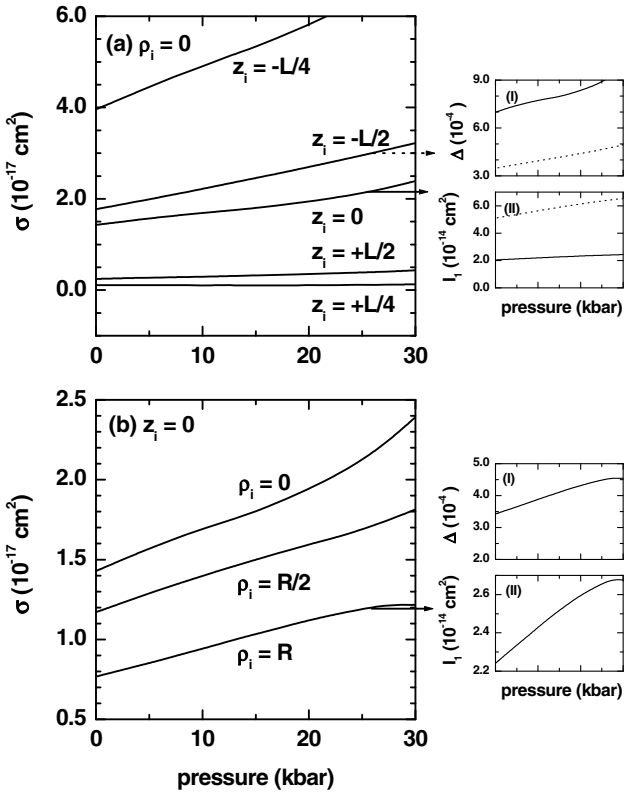

Fig. 5. Donor impurity related photoinization cross section in cylindrical-shape GaAs-(Ga, Al)As quantum dot (R = 100 Å, L = 200 Å) as a function of the hydrostatic pressure and for parallel polarization (with respect to the z-axis of the dot) of the incident radiation. The results are for B = 10 T and F = 10 kV/cm. The impurity is shifted along the axial (a) and radial (b) direction of the dot. In each curve for the energy of the incident photon we take $\hbar\omega = E_b|_{P=0}$. The lateral Figures 1 and 2 are, according with equations (16) and (17), for the pressure dependence of *Delta* and I_1 for impurities located at $(0, 0)$, $(-L/2, 0)$, and $(0, R)$.

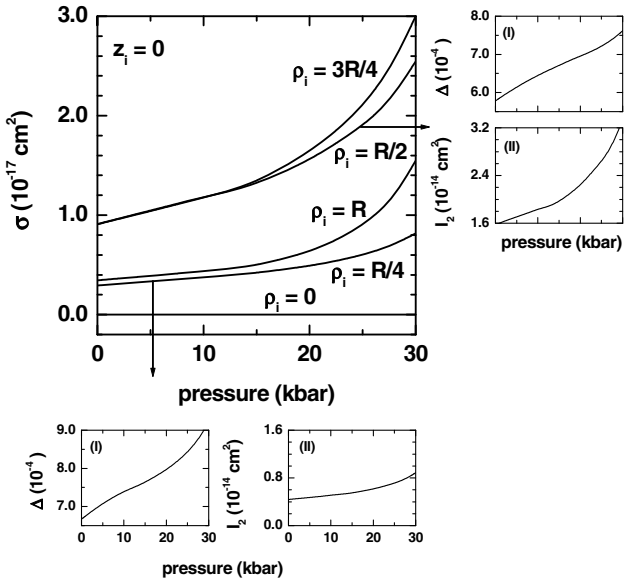

Fig. 6. Donor impurity related photoinization cross section in cylindrical-shape GaAs-(Ga, Al)As quantum dot (R = 100 Å, L = 200 Å) as a function of the hydrostatic pressure and for perpendicular polarization (with respect to the z-axis of the dot) of the incident radiation. The results are for B = 10 T and F = 10 kV/cm. The impurity is shifted along the radial direction of the dot. In each curve for the energy of the incident photon we take $\hbar\omega = E_b|_{P=0}$. Figures 1 and 2 in the right and bottom panels are, according with equations (16) and (18), for the pressure dependence of Δ and I_2 for impurities located at $(0, R/2)$ and $(0, R/4)$.

of the impurity position. For the calculations that led to those figures, we supposed that the energy of the incident photon is equal to the impurity binding energy at zero pressure. In all the cases considered, the PCS increases with increasing pressure, and this is due to the linear increasing of the electron effective mass, see equations (2), (12) and (13); inspection of the curves reveals that for smaller values of the impurity coordinate this behavior is larger, because the electron is more localized and in these conditions the influence of the hydrostatic pressure effect is bigger. From Figure 5 it is clear that the PCS increases (decreases) when the impurity is shifted towards the $-z$ ($+z$) direction. This effect is dominated by the expectation value of z between the initial and final states, represented by I_1 in equation (17) and depicted in the lateral Figure 2. Note that as effect of the electric field the electron is pushed towards the impurity when z_i is negative and far from the impurity when z_i is positive. Finally, when the impurity is shifted along the radial direction the PCS decreases mainly due to the diminishing in the Δ-parameter represented in equation (16) and depicted in the lateral Figure 1.

Our calculation for the effect of the hydrostatic pressure on the PCS for different values of radial-impurity coordinate for perpendicular polarization of the incident radiation is displayed in Figure 6. Again, for the calculations that led to this figure, we supposed that the energy of the incident photon is equal to the impurity binding energy at zero pressure. Again, the PCS increases with increasing pressure, as happened in Figure 5. This effect is mainly associate to the increasing of the Δ-parameter with the hydrostatic pressure, as is shown in Figure 1. According with the increasing of the effective mass with the hydrostatic pressure, there is an increasing in the Γ-parameter – equation (14) – and finally in the Δ-parameter. For P = 30 kbar and for radial impurity positions lower than $3R/4$, the PCS is a growing function with the increasing of ρ_i due to the increasing of the expectation value of $\rho\cos\varphi$ between the initial and final states, as can be observed by comparing the results for I_2 in the two lateral Figure 2. For $\rho_i = R$ the PCS decreases mainly due to the increasing of the binding energy. In this case, because the barrier height is close to zero, the electron wavefunction is almost symmetrical around the impurity position with the corresponding increasing in the Coulomb interaction. A similar increasing and decreasing behavior with the impurity position is observed at $P = 0$. Note that in accordance with equation (18), the PCS is exactly zero for $\rho_i = 0$.

4 Conclusions

We studied the behavior of the donor-impurity related binding energy and PCS in a cylindrical-shape QDs, under the effects of hydrostatic pressure and in-growth direction applied electric and magnetic fields. In our calculations we used the effective mass and parabolic bands approximations within a variational scheme. Several values for the structure dimensions were considered, too. Our results show that in the regime of low pressure (less than the corresponding value to the $\Gamma - X$ crossover for the barrier material) the impurity binding energy growths linearly with the pressure. We also showed that in the high pressure regime (larger than the corresponding value to the $\Gamma - X$ crossover for the barrier material) the binding energy growths up to reach a maximum and then decreases. We additionally found that the applied electric and magnetic fields may favor the increase or decrease in the binding energy, depending of the impurity position. Also, we found that for the parallel and perpendicular polarization of the incident radiation, the PCS growths with the hydrostatic pressure. Our results suggest that for parallel polarization of the incident radiation, the PCS can increases or decreases depending of the axial direction along which the impurity is shifted from the center of the dot. In this case of parallel polarization, the PCS always decreases with radial displacements of the impurity. In the case of perpendicular polarization of the incident radiation, the PCS is a complicated function of the impurity position along the radial direction of the dot showing that the PCS decreases when the impurity is placed close to the axis of the dot or near to the cylindrical boundary. Both for parallel and perpendicular polarizations of the incident radiation, the PCS drops to zero when the axial or radial symmetries are preserved, respectively.

C.A.D. is grateful with Dr. Anna Kurczyńska for valuable comments and suggestions. This work was partially financed by COLCIENCIAS-Colombia, CODI-Universidad de Antioquia (Estrategia de Sostenibilidad Grupo de Materia Condensada-UdeA, 2009–2010), and Facultad de Ciencias Exactas y Naturales-Universidad de Antioquia (CAD: project of exclusive dedication 2009–2010). A.A.K. would like to thank the Armenian State Program on Semiconductor Nanoelectronics.

References

1. G. Bastard, Phys. Rev. B **24**, 4714 (1981)
2. J.H. Burnett, H.M. Cheong, W. Paul, E.S. Koteles, B. Elman, Phys. Rev. B **47**, 1991 (1993)
3. A.M. Elabsy, Superlatt. Microstruct. **14**, 65 (1993)
4. A.M. Elabsy, J. Phys.: Condens. Matter **6**, 10025 (1994)
5. J.G. Tischler, H.A. Nickel, B.D. McCombe, B.A. Weinstein, A.B. Dzyubenko, A.Y. Sivachenko, Physica E **6**, 177 (2000)
6. A.L. Morales, A. Montes, S.Y. López, C.A. Duque, J. Phys.: Condens. Matter **14**, 987 (2002)
7. A.J. Peter, K. Navaneethakrishnan, Superlatt. Microstruct. **43**, 63 (2008)
8. E.C. Niculescu, L.M. Burileanu, A. Radu, Superlatt. Microstruct. **44**, 173 (2008)
9. E. Kasapoglu, Phys. Lett. A **373**, 140 (2008)
10. H.T. Cao, D.B. Tran Thoai, Physica B **205**, 273 (1995)
11. S. Aktas, F.K. Boz, S.S. Dalgic, Physica E **28**, 96 (2005)
12. O. Akankan, S.E. Okan, H. Akbas, Physica E **36**, 119 (2007)
13. S. Aktas, A. Bilekkaya, S.E. Okan, Physica E **40**, 2703 (2008)
14. E. Kasapoglu, H. Sari, I. Sökmen, Physica B **353**, 345 (2004)
15. N. Raigoza, C.A. Duque, N. Porras-Montenegro, L.E. Oliveira, Physica B **371**, 153 (2006)
16. C.A. Duque, A. Montes, A.L. Morales, N. Porras-Montenegro, J. Phys.: Condens. Matter **9**, 5977 (1997)
17. A. Zounoubi, I. Zorkani, K. El Messaoudi, A. Jorio, Phys. Lett. A **312**, 220 (2003)
18. C. Xia, F. Jiang, S. Wei, X. Zhao, Microelectronics Journal **38**, 663 (2007)
19. S.T. Pérez-Merchancano, H. Parédes-Gutierrez, J. Silva-Valencia, J. Phys.: Condens. Matter **19**, 026225 (2007)
20. Z. Zhao, J. Zeng, Z.J. Ding, X.P. Wang, J.G. Hou, Z.M. Zhang, J. Appl. Phys. **102**, 053509 (2007)
21. C. Xia, Y. Liu, S. Wei, Appl. Surface Science **254**, 3479 (2008)
22. C. Xia, F. Jiang, S. Wei, Superlatt. Microstruct. **43**, 285 (2008)
23. F. Jiang, C. Xia, S. Wei, Physica B **403**, 165 (2008)
24. F.C. Jiang, C. Xia, Y.M. Liu, S.Y. Wei, Physica E **40**, 2714 (2008)
25. C. Dane, H. Akbas, S. Minez, A. Guleroglu, Physica E **41**, 278 (2008)
26. A.L. Vartanian, L.A. Vardanyan, E.M. Kazaryan, Phys. Stat. Sol. (b) **245**, 123 (2008)
27. R.B. Santiago, L.E. Oliveira, J. d'Albuquerque e Castro, Phys. Rev. B **46**, 4041 (1992)
28. H.O. Oyoko, N. Porras-Montenegro, S.Y. López, C.A. Duque, Phys. Stat Sol. (c) **4**, 298 (2007)
29. M. de Dios-Leyva, E.Z. da Silva, L.E. Oliveira, J. Appl. Phys. **76**, 3217 (1994)
30. A. Latgé, N. Porras-Montenegro, L.E. Oliveira, Phys. Rev. B **51**, 13344 (1995)
31. A. Bruno-Alfonso, L.E. Oliveira, M. de Dios-Leyva, Appl. Phys. Lett. **67**, 536 (1995)
32. C.A. Duque, A. Montes, N. Porras-Montenegro, L.E. Oliveira, J. Phys. D: Appl. Phys. **32**, 3111 (1999)
33. S.Y. López, N. Porras-Montenegro, C.A. Duque. Physica B **362**, 41 (2005)
34. M. de Dios-Leyva, C.A. Duque, L.E. Oliveira, Phys. Rev. B **76**, 075303 (2007)
35. L.E. Oliveira, M. de Dios-Leyva, C.A. Duque, Microelectron. J. **39**, 398 (2008)
36. A.L. Morales, N. Raigoza, C.A. Duque, L.E. Oliveira, Phys. Rev. B **77**, 113309 (2008)
37. M. Takikawa, K. Kelting, G. Brunthaler, M. Takeshi, J. Komena, J. Appl. Phys. **65**, 3937 (1989)
38. M. El-Said, M. Tomak, Solid State Commun. **82**, 721 (1992)
39. J.D. Correa, N. Porras-Montenegro, C.A. Duque, Phys. Stat. Sol. B **241**, 2440 (2004)

40. E. Kasapoglu, U. Yesilgül, H. Sari, I. Sökmen, Physica B **368**, 76 (2005)
41. V.N. Mughnetsyan, M.G. Barseghyan, A.A. Kirakosyan, Physica E **40**, 654 (2008)
42. A. Sali, M. Fliyou, H. Satori, H. Loumrhari, J. Physics Chemistry of Solids **64**, 31 (2003)
43. V.N. Mughnetsyan, M.G. Barseghyan, A.A. Kirakosyan, Superlatt. Microstruct. **44**, 86 (2008)
44. A. Sali, H. Satori, M. Fliyou, H. Loumrhari, Phys. Stat. Sol. (b) **232**, 209 (2002)
45. H. Ham, C.J. Lee, J. Korean Phys. Soc. **42**, S688 (2003)
46. H. Ham, H.N. Spector, J. Appl. Phys. **93**, 3900 (2003)
47. J.D. Correa, O. Cepeda-Giraldo, N. Porras-Montenegro, C.A. Duque, Phys. Stat. Sol. (b) **241**, 3311 (2004)
48. J.D. Correa, N. Porras-Montenegro, C.A. Duque, Braz. J. Phys. **36**, 387 (2006)
49. M. Şahin, Phys. Rev. B **77**, 045317 (2008)
50. M.G. Barseghyan, A.A. Kirakosyan, C.A. Duque, Phys. Stat. Sol. (b) **246**, 626 (2009)
51. N. Raigoza, A.L. Morales, A. Montes, N. Porras-Montenegro, C.A. Duque. Phys. Rev. B **69**, 045323 (2004)
52. A.M. Elabsy, Phys. Rev. B **46**, 2621 (1992); Z.Y. Deng, T.R. Lai, J.K. Guo, Phys. Rev. B **50**, 5732 (1994)
53. T. Ando, H. Akera, Phys.Rev. B **40**, 11619 (1989)
54. J.P. Cuypers, W. van Haeringen, Phys. Rev. B **48**, 11469 (1993)
55. M.E. Mora-Ramos, S.Y. López, C.A. Duque, V.R. Velasco, Phys. Stat Sol. (c) **4**, 418 (2007)
56. C.A. Duque, S.Y. López, M.E. Mora-Ramos, Phys. Stat. Sol. (b) **244**, 1964 (2007)
57. M.E. Mora-Ramos, S.Y. López, C.A. Duque, Physica E **40**, 1212 (2008)
58. M.E. Mora-Ramos, S.Y. López, C.A. Duque, Eur. Phys. J. B **62**, 257 (2008)
59. O. Oubram, M.E. Mora-Ramos, L.M. Gaggero-Sager, Eur. Phys. J. B **71**, 233 (2009)
60. P.Y. Yu, M. Cardona, *Fundamentals of Semiconductors* (Springer-Verlag, Berlin, 1996)
61. S.-L. Chuang, S.S. Rink, D.A.B. Miller, D.S. Chemla, Phys. Rev. B **43**, 1500 (1991); B. Yoo, B.D. McCombe, W. Schaff, Phys. Rev. B **44**, 13152 (1991); M. Cai, W. Liu, Y. Liu, Phys. Rev. B **46**, 4281 (1992); Y.-P. Feng, H.N. Spector, Phys. Rev. B **48**, 1963 (1993); A. Latgé, N. Porras-Montenegro, L.E. Oliveira, Phys. Rev. B **51**, 2259 (1995); E.C. Niculescu, Mod. Physics Lett. B **14**, 1073 (2000)
62. D.S. Chemla, J. Lumin. **30**, 502 (1985)